48th AIAA Aerospace Sciences Meeting Including the New Horizons Forum and Aerospace Exposition
4 - 7 January 2010, Orlando, Florida

AIAA 2010-47

Effect of Dynamic Pressure on Direct Shear Stress Sensor Design

Vijay Chandrasekharan,[1] Jeremy Sells,[2] David P. Arnold,[3] and Mark Sheplak[4]
Interdisciplinary Microsystems Group, University of Florida, Gainesville, FL, 32611

A microelectromechanical systems (MEMS)-based capacitive floating element shear stress sensor, developed for time-resolved turbulence measurement, is studied for its response to unsteady pressure forcing. The floating element structure incorporates interdigitated comb fingers forming differential capacitors, which provide electrical output proportional to the floating element deflection. An equivalent circuit model is provided under simultaneous pressure and shear loading. A design strategy to mitigate pressure sensitivity while enhancing shear stress sensitivity is provided. The significance of the design methodology is experimentally illustrated via comparison of combined shear and pressure response of the sensor with its pressure response. Results indicate a significant effect of pressure on combined sensor response despite 64 dB of pressure rejection.

I. Introduction

The measurement of time-resolved wall shear stress is important for fundamental study of fluid mechanics, aerodynamic design, validation of computational techniques and flow control applications. Quantitative wall shear stress information is vital for development of more efficient aircraft and space vehicles. One challenge involved in making quantitative, time resolved wall shear stress measurements requires sensors that are sensitive to shear stress but insensitive to pressure fluctuations in the flow.

MEMS shear stress sensors may be broadly classified as direct and indirect shear stress sensors. While indirect sensors rely on a correlation between the measured flow property and shear stress, direct sensors measure the integrated shear stress on the sensor surface. Micromachined indirect shear stress sensors such as thermal sensors,[1-4] micro-fences,[5] micro-pillars,[6, 7] and laser based sensors [8, 9] have been previously reported in literature. Capacitive,[10-16] optical,[17-20] and piezoresistive,[21-24] transduction schemes have been commonly used for direct shear stress sensors. Every research effort represented a progress towards shear stress measurement, but had performance limitations due to sensitivity drift, insufficient dynamic range, bandwidth, and/or high minimum detectable signal (MDS). The University of Florida has recently developed a capacitive sensor with performance specifications suitable for turbulence measurement applications. In this paper, the sensitivity of this device to unsteady pressure forcing is explored. [16] Pressure insensitivity is very important for shear stress sensors, since the pressure forces in a turbulent flow can roughly be an order of magnitude higher than the shear forces.[25] Previous research efforts have focused on static pressure mitigation[10, 26], but the mitigation of dynamic/ac pressure has not been formally addressed. Careful investigation of pressure rejection is critical and needs greater efforts to develop a fully characterized direct shear stress sensor. The focus of this work is to develop models to facilitate better design of direct shear stress sensors in general and for a capacitive sensor in particular along with some preliminary results for estimating shear stress sensor behavior under pressure loading.

A floating element sensor structure with a sensing element, compliant tethers, and interdigitated capacitive comb fingers is utilized. Change in gap between the capacitive electrodes due to shear induced sensor deflection produces

[1] Research Associate, Department of Mechanical and Aerospace Engineering, 231 MAE-A, Gainesville, FL, 32611-6250.

[2] Graduate Research Assistant, Department of Electrical and Computer Engineering, 231 Benton Hall, Gainesville, FL, 32611-6250.

[3] Assistant Professor of Electrical and Computer Engineering, 229 Benton Hall, Gainesville, FL 32611-6250.

[4] Professor of Mechanical and Aerospace Engineering, AIAA Associate Fellow, 231 MAE-A, Gainesville, FL 32611-6250.

Vijay Chandrasekharan, Jeremy Sells, David Arnold, and Mark Sheplak. "Effect of Dynamic Pressure on Direct Shear Stress Sensor Design", 48th AIAA Aerospace Sciences Meeting Including the New Horizons Forum and Aerospace Exposition, Aerospace Sciences Meetings, https://doi.org/10.2514/6.2010-47

an output voltage under an appropriate bias voltage via capacitive transduction. Figure 1 shows a schematic of the sensor illustrating various dimensions. The bias voltage establishes a constant charge across the capacitors. Consequently, a change in capacitance due to sensor motion results in a voltage change given as

$$V = \frac{Q|_{\text{constant}}}{C}, \tag{1}$$

where V is the voltage across the capacitors, Q is the charge, which is held constant by the voltage biasing scheme, and C is the sense capacitance. The differential capacitance measurement scheme, which is widely used in inertial sensors is utilized.[27] A pair of matched capacitors (ideal) formed in the sensor structure are biased with identical voltages of opposite polarity to form a voltage divider or balanced capacitive half bridge (Figure 2). The voltage at the middle node is thus zero and remains at zero for a balanced bridge or identical capacitance change.[27] A finite voltage results at the middle node due to a bridge imbalance resulting from a difference in the sense capacitances.

The voltage output (directly proportional to shear stress) is read using a voltage buffer, SiSonic™.[28] Ideally, shear induced in-plane sensor motion results in a differential signal producing a voltage, whereas a pressure induced out-of-plane sensor motion results in a common mode signal with no resultant voltage output. The out-of-plane mechanical stiffness and differential capacitance measurement scheme were initially implemented to mitigate pressure sensitivity of the sensor. This paper will highlight some of the non-idealities and their effects on the dynamic pressure response of the sensor. Sensor design concept (independent of transduction scheme) to further mitigate sensor pressure sensitivity is also illustrated.

The remainder of the paper is organized as follows. A brief overview of sensor modeling concept for pressure response is given in Section II, along with relevant mathematical expressions. The experimental setup is described in Section III. Section IV summarizes some preliminary characterization results while pointing to necessity for the inclusion of sensor pressure sensitivity during the modeling process. Finally, conclusions and planned future work are given in Section V.

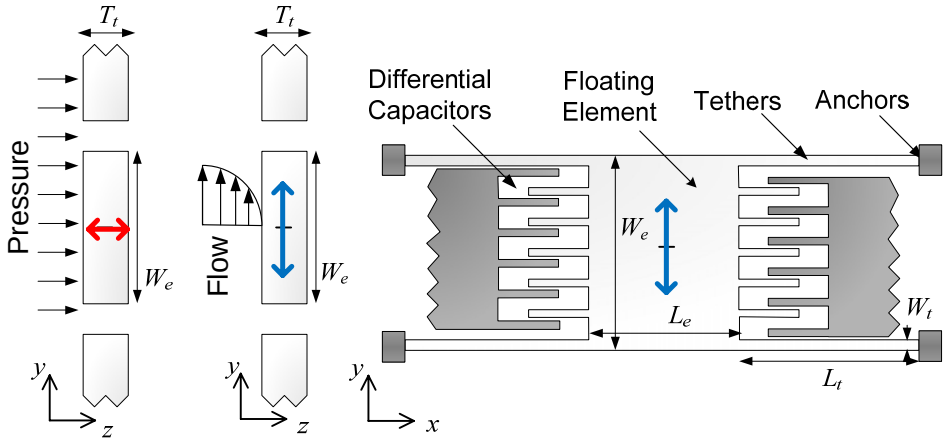

Figure 1 Schematic of geometry of differential capacitive shear stress sensor.

II. Sensor Design

This section provides an overview of the shear stress sensor structure and the sensor design concept for simultaneous shear and pressure loading. A system-level physical model is developed that may be divided into three parts: mechanical model (shear and pressure), electrical model, and equivalent electromechanical circuit model.

A. Mechanical Modeling

The sensor mechanical model establishes the relation between the shear stress, τ_w and pressure p_{in}, and the corresponding floating element deflections, δ_τ (shear) and δ_p (pressure), respectively. The sensitivities, bandwidths, linearity and dynamic responses of the sensor under both shear and pressure forcing are strong functions of the sensor structural design. The modeling and theoretical basis for the sensor motion were previously published elsewhere.[29] The deflection of the floating element under the influence of shear stress is given as[29]

$$\delta_\tau = \frac{\tau_w W_e L_e}{4ET_t}\left(1+\frac{NW_f L_f}{W_e L_e}+2\frac{W_t L_t}{W_e L_e}\right)\left(\frac{L_t}{W_t}\right)^3. \quad (2)$$

Here, L_e and W_e are the length and width of the floating element; L_t and W_t are length and width of the tethers; L_f and W_f are the length and width of the comb fingers; T_t is the thickness of the floating element, tethers and comb fingers; N is the number of comb fingers; and E is the Young's modulus of the sensor material (in this case silicon). One of the measures to minimize pressure rejection structurally is to ensure $T_t >> W_t$ to enable higher stiffness in the transverse direction, minimizing out-of-plane motion. Pressure forcing, p_{in}, causes a transverse deflection, δ_p, given as

$$\delta_p = \frac{p_{in} W_e L_e}{4EW_t}\left(1+\frac{NW_f L_f}{W_e L_e}+2\frac{W_t L_t}{W_e L_e}\right)\left(\frac{L_t}{T_t}\right)^3. \quad (3)$$

The sensor's sensing area remains unaltered for pressure loading, however the stiffness is higher in the transverse direction by $(W_t/T_t)^2$. This aspect ratio limits both the in-plane and out-of-plane stiffnesses and is constrained by the limitations of the etch use to define the tethers during the fabrication process.

B. Electrical Modeling and Interface Circuit

The capacitive electrodes formed by the comb fingers and other overlapping surfaces on the sensor are modeled as parallel plate capacitors while neglecting fringing field capacitance.[29] A voltage amplifier with a constant charge biasing scheme serves as the electrical circuit necessary to get a voltage read-out proportional to the capacitance change (Figure 2). The bias resistor R_b sets the amplifier dc operating point, C_p is the parasitic capacitance, and C_i is the input capacitance of the amplifier. The instantaneous sensor capacitances represented as C_1 and C_2 at the input of the interface circuit are biased with equal voltages of opposite polarity. These capacitances change due to sensor motion resulting from both shear stress and pressure. The output voltage for this configuration is,[27]

$$V_{out} = V_B \frac{C_1 - C_2}{C_1 + C_2 + C_p + C_i}. \quad (4)$$

While the shear stress input results in a differential signal, a pressure input serves as a common mode signal with ideally no output. For shear stress induced in-plane sensor displacement in the y-direction, C_1 increases $(C_0 + \Delta C)$ and C_2 decreases $(C_0 - \Delta C)$ or vice-versa. This results in a differential output voltage,

$$V_{out}\big|_{differential} = \frac{\Delta C}{C_0 + (C_p + C_i)/2} \quad (5)$$

Pressure induced out-of-plane motion in the z-direction causes simultaneous increase/decrease of C_1 and C_2, $(C_0 \pm \Delta C)$, resulting in no voltage output. The high stiffness along the x-direction (axial loading) allows neglecting voltage output due to sensor motion in that direction.

The discussion so far considered the ideal case of matched sensor capacitances for pressure rejection using the differential capacitance sensing strategy. However, now consider a non-ideal case for the sensor when there exists a slight mismatch between C_1 and C_2. For instance, assume the nominal sensor capacitances are mismatched such that, $C_{20} = \lambda C_{10} = \lambda C_0$, where λ is the mismatch factor. The deflection δ_p due to an applied pressure input p_{in}

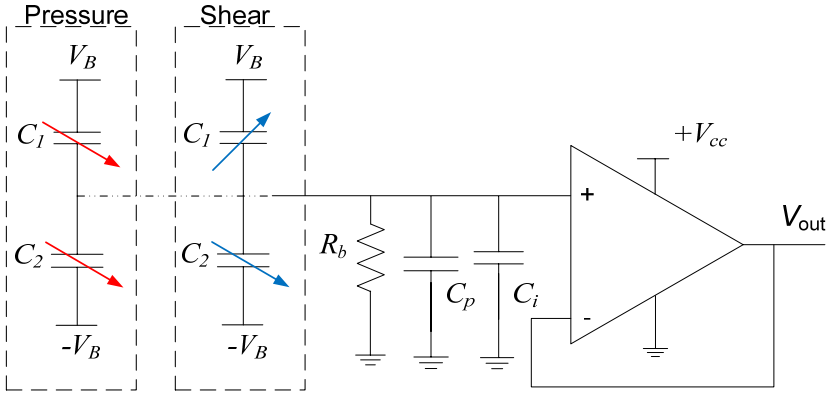

Figure 2 Schematic of the readout concept using a voltage amplifier showing the effect of both shear and pressure.

on the sensor results in a change in the overlapping area of the capacitive electrodes. This results in a linear change in the sense capacitances which, simultaneously increase or decrease. Thus, for change in capacitance ΔC for C_1, the corresponding change in C_2 is $\lambda\Delta C$. Therefore the instantaneous capacitance values are

$$C_1 = C_0 + \Delta C \tag{6}$$

and

$$C_2 = \lambda\left(C_0 + \Delta C\right). \tag{7}$$

Using Eq.(5), the resulting output voltage is written as

$$V_{out}\big|_{pressure} = \frac{\left(1-\lambda\right)\left(C_0 + \Delta C\right)}{\left(1+\lambda\right)\left(C_0 + \Delta C\right) + C_p + C_i}. \tag{8}$$

This shows that a finite output voltage which scales with the mismatch factor λ is obtained under pressure loading. Since, the differential measurement scheme relies on matched sense capacitors, other mitigation strategies are important to further improve pressure rejection.

C. Equivalent Electromechanical Circuit Model

The transduced electrical output due sensor mechanical motion is modeled using a transformer—a two-port circuit element, generally used in transducer modeling.[27] The distributed mechanical system is represented using lumped elements such as lumped mass, compliance, and resistance using lumped element modeling (LEM) technique. Figure 3 shows the equivalent circuit representation of the sensor under simultaneous shear and pressure forcing. The assumptions required to model the system in Figure 3 are: no coupling between in-plane and out-of-plane modes of the sensor structure, weak electromechanical coupling, infinite (ideal) amplifier input impedance, and an electronic bandwidth much higher than that of the sensor mechanical response (shear and pressure). Thus the mechanical response of the sensor in both shear and pressure dominates the entire system response.

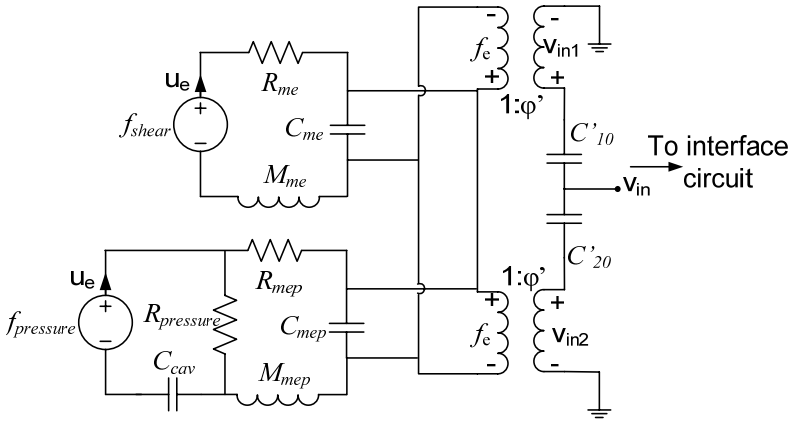

Figure 3 Schematic of equivalent circuit for the differential capacitive shear stress sensor.

The lumped mechanical mass and compliance of the sensor in shear are C_{me} and M_{me} while C_{mep} and M_{mep} are the corresponding lumped parameters for pressure. Compliances represent potential energy storage in compliant deflected tethers and lumped masses represent kinetic energy storage due to structural motion. Finite damping/resistance due to flow through the gaps and underneath the sensor structure are represented by R_{me} and R_{mep} respectively. Assuming an under-damped second order system for the sensor motion under both shear and pressure forcing, the effects of R_{me} and R_{mep} are limited to the upper end of the sensor response and are neglected for modeling simplicity. The relevant mathematical expressions for the lumped parameters were given in a previous publication.[29] Neglecting attenuation, the independent static sensitivities of the sensor for shear and pressure are

$$\mathrm{S}_{shear} = V_B \frac{\delta_\tau / \tau_w}{g_{01}} \tag{9}$$

and

$$\mathrm{S}_{pressure} = V_B \frac{\delta_p / p_{in}}{T_t}, \tag{10}$$

where g_{01} is the initial gap of interest between the capacitive electrodes and the tether thickness T_t is the initial overlap between the electrodes for pressure induced motion.

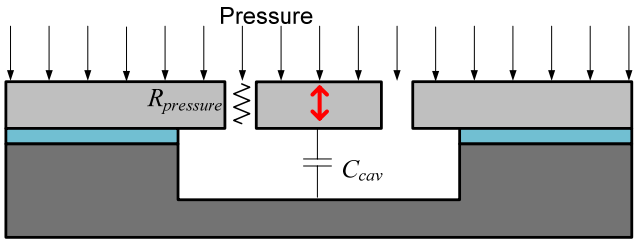

Figure 4 Cross section indicating lumped parameters due to cavity underneath the sensor.

There exists a cavity underneath the sensor (Figure 4), which has an associated compliance / stiffness, C_{cav}, due to the compressibility of the fluid in it. In a lumped sense, the cavity compliance opposes the out-of-plane motion of the sensor referred to as the cavity stiffening. The attenuation of the pressure induced sensor output due to cavity stiffening is

$$H_{cavity} = \frac{C_{cav}}{C_{cav} + C_{mep}}. \tag{11}$$

In addition to this, the back cavity is vented to the atmosphere through the gaps around the sensor, which are necessary for the sensor fabrication process. The vent offers a resistance, $R_{pressure}$, to the fluidic flow across the sensor thickness between the front and back side. Squeeze film damping also adds to this resistance and is a function of the film thickness under the cavity. This damping becomes important as the cavity is made shallower to increase the cavity stiffening effect. The cavity compliance and the vent resistance form a high pass filter with a corner frequency of

$$f_{cut-on} = \frac{1}{2\pi\sqrt{R_{pressure}C_{cav}}}. \tag{12}$$

Microphone designers commonly design the compliance and the vent resistor to have a low cut-on frequency in complex vented perforated structures using combination of perforate resistance and squeeze film damping.[30-32] In contrast, in a shear stress sensor, these should be designed to move this cut-on frequency beyond the operating bandwidth for shear stress. This modeling aspect has not been explored previously and could greatly benefit floating element shear stress sensor design.

III. Experimental Setup

This section explains the experimental setup to characterize the sensor pressure response and later compared with its frequency response with combined shear and pressure inputs. Silicon micromachining fabrication process results in sensors with a total die size of $5\,mm \times 5\,mm$. Figure 5 shows a picture of the sensor and a schematic of the interface circuit connections. The sensor is epoxied in a recessed printed circuit board (PCB) such that it is flush with the surface, which in turn is mounted in a recessed Lucite plug for testing. The amplifier (SiSonic™) is placed on the back side of the PCB in close proximity to the sensor (Figure 6) to minimize parasitic attenuation arising from the connection traces on the PCB. The packaged sensor is characterized for dynamic pressure sensitivity, pressure frequency response and combined pressure and shear frequency response in the plane wave tube (PWT).

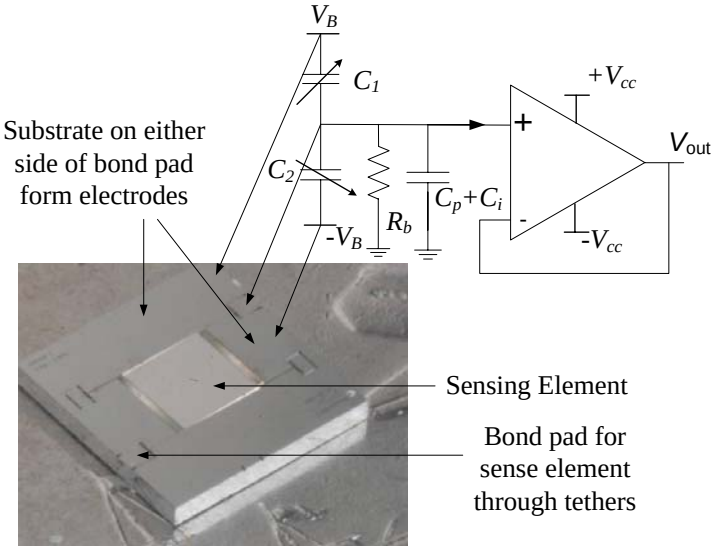

Figure 5 Schematic with optical image of sensor die ($5\,mm \times 5\,mm$) indicating floating element, contact pads, and interface circuit (voltage buffer).

A. Dynamic Characterization

Plane waves generated by a BMS 4590P compression driver (speaker), mounted at one end of the PWT, propagate along the length of the tube. The PWT consists of a square duct, 1"×1" in cross section, which has a cut-on of 6.7 *kHz* frequency for higher order acoustic modes. Figure 7 shows the schematic of the experimental setup for studying sensor response with dynamic pressure forcing. Figure 8 shows the experimental setup for measuring the sensor response under simultaneous shear and pressure forcing. For pressure characterization, the packaged sensor is mounted on a rigid plate is mounted at the end of the PWT to test its pressure response via normal acoustic incidence. A 1/8" B&K Type 4138 reference microphone is used to monitor the pressure at the termination or sensor plane. For simultaneous shear and pressure forcing, the PWT is fitted with an anechoic termination (30.7" long fiber glass wedge) to enable plane progressive waves, which minimizes acoustic reflections. The sensor and a references microphone are mounted on the sidewall on the same axial plane along the length of the tube (Figure 8). The sensor is biased with a differential $10\,V$ dc bias for these experiments. A B&K PULSE Multi-Analyzer System (Type 3109) acts as the microphone power supply, data acquisition unit, and signal generator for the compression driver. The data from combined frequency response (shear and pressure) is compared with the measured pressure frequency response.

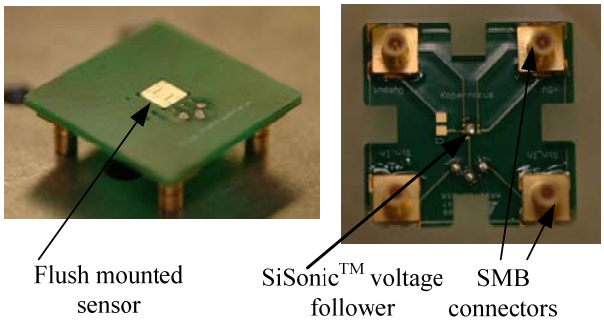

Figure 6 Photographs of sensor packaged on a $30\,mm \times 30\,mm$ PCB board and inserted into the lucite plug.

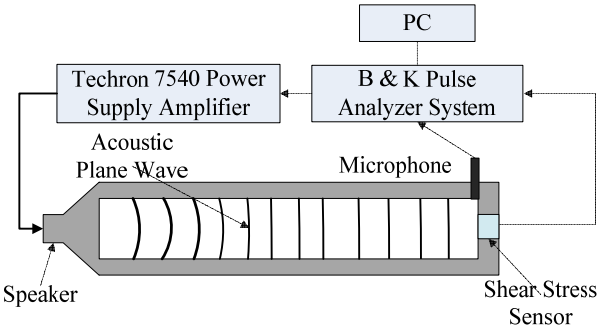

Figure 7 A schematic of the dynamic calibration setup for measuring pressure sensitivity using normal incidence acoustic waves.

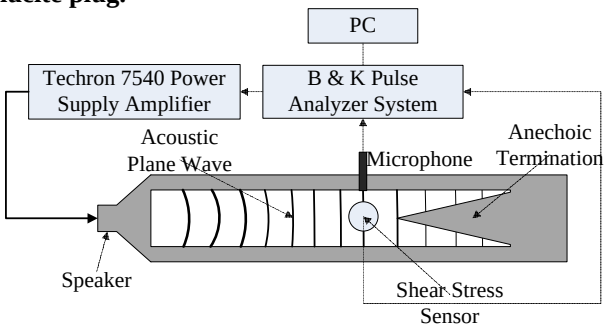

Figure 8 A schematic of the dynamic calibration setup for combined shear stress and pressure frequency response with plane progressive acoustic waves.

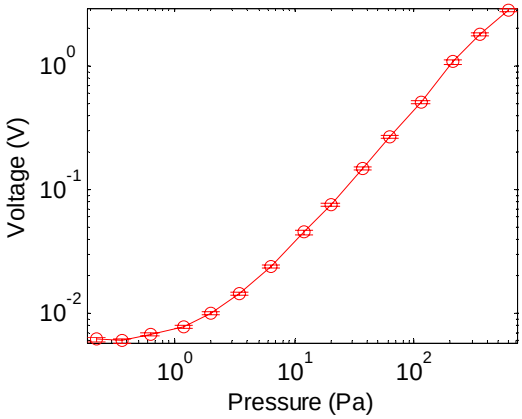

Figure 9 Sensor voltage output as a function of pressure using normal acoustic incidence in PWT at $V_B = 10\,V$ and $f = 4.2\,kHz$.

IV. Results and Discussion

A. Characterization Results

During characterization the sensor pressure sensitivity and pressure response of the sensor as a function of frequency are first tested. The sensor response as a function of frequency is compared for only pressure input and

combined shear and pressure inputs. Since the absolute levels of the combined shear and pressure measurements are to be compared with those of pure pressure inputs, the input conditions for both frequency response measurements are kept identical to maintain a constant shear stress given as,[33]

$$\tau_{in} = -\frac{p'\sqrt{j\omega\nu}}{c} e^{j(\omega t - kx_0)} \tanh\left(a\sqrt{\frac{j\omega}{\nu}}\right), \tag{13}$$

where ν is the kinematic viscosity of air, c is the isentropic speed of sound or wave speed, $k = \omega/c$ is the acoustic wave number and a is the duct width.

The sensor is tested for its pressure sensitivity under normal acoustic incidence, where the pressure is increased from $80\,dB$ to $160\,dB$ (ref $20\,\mu Pa$) at a constant frequency of $4.2\,kHz$. The results from this calibration shown in Figure 9 indicate a pressure sensitivity of $4.8\,\mu V/Pa$, which is a pressure rejection of $64\,dB$ when compared to a shear sensitivity of $7.66\,mV/Pa$. The sensor response as a function of frequency for simultaneous shear and pressure forcing is conducted for a constant theoretical input shear stress $|\tau_{in}| = 0.5\,Pa$ using the anechoic termination with the PWT. Figure 10 shows the sensor frequency response which is computed as

$$H(f) = \left(\frac{V(f)}{\tau_{in}(f)}\right)\frac{\partial\bar{\tau}}{\partial\bar{V}} \tag{14}$$

where $V(f)$ is the sensor output voltage, $\tau_{in}(f)$ is the input shear stress, $\partial\bar{\tau}/\partial\bar{V}$ is the inverse of the sensor shear stress sensitivity previously estimated as $7.66\,mV/Pa$. The sensor exhibits a classical second order frequency response with resonance at $6.2\,kHz$ captured in both magnitude and phase. Despite significant pressure rejection it is suspected that the sensor response is also affected by the input acoustic pressure. Therefore, the frequency response measurements using the anechoic termination are considered only qualitative. This is further illustrated by comparing the frequency response functions (FRF), H_{ms}, between the sensor and reference microphone for pure pressure forcing and the combined shear and pressure forcing. The FRF between the sensor and the microphone for the two cases are as shown in Figure 11.

A higher, combined pressure-shear frequency response indicates that despite similar and higher pressure forces, the sensor remains more sensitive to shear in the frequency range of measurement than it is to pure pressure. The scatter in the pressure data is due to the poor performance of the sensor for pressure inputs. Note, that the sensor was not designed for pressure measurements and relies purely on the capacitance mismatch (ideally zero) for this measurement. Similar qualitative nature of the two magnitude responses may be due to the shaping of the overall frequency response by the pressure response of the sensor. Also, for out-of-plane motion of the sensor, close to its in-plane resonance frequency, a small perturbation in the in-plane direction may be sufficient to excite its in-plane

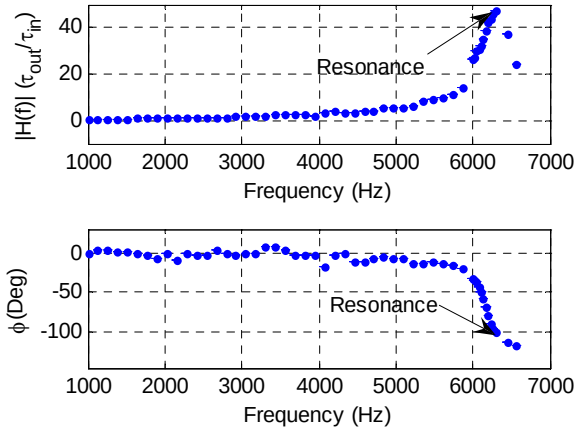

Figure 10 Frequency response of sensor at $V_B = 10\,V$ using $|\tau_{in}| = 0.5\,Pa$ as the reference input.

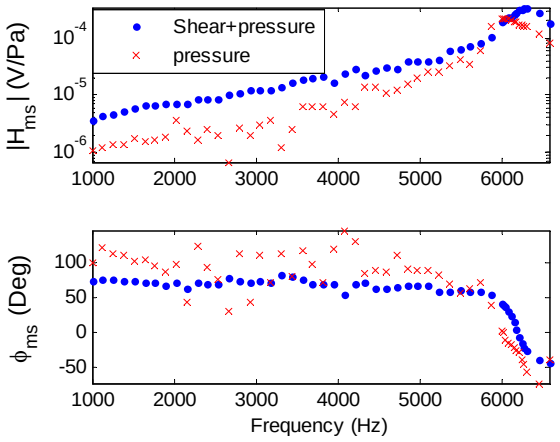

Figure 11 Comparison of combined (shear and pressure) and pressure frequency response measured between sensor and reference microphone.

resonant motion. An FEA simulation was performed to ensure that the pressure and shear resonances of mechanical structure are not in close proximity. The results reveal that the first mode, which is the in-plane mode, is at $5.2\,kHz$ and the second mode, which is the out-of-plane mode, is at $14.4\,kHz$. These values are to within 4 % of the LEM predictions. Thus, for better understanding of the sensor performance a lumped element model with combined shear and pressure inputs is necessary, including the effects of cavity stiffening and the cut-on frequency for pressure.

With these observations, the design of direct floating element based shear stress sensors requires constraints that improve shear stress response while attenuating pressure response. The schematic in Figure 12 shows the desirable region of operation for the sensor under both shear and pressure forcing. The figure indicates that the sensor should be designed so as to maximize the sensor operation range under shear stress and use the combination of structural stiffness, common mode rejection, cavity stiffening effect, and tuning of f_{cut-on}, which high pass filters the pressure response beyond the desirable sensor shear bandwidth. Such a design approach will significantly raise the sensor minimum detectable signal (MDS) for pressure and simultaneously also make it unresponsive to pressure in the frequency range of interest for shear stress measurement. A multi objective optimization to maximize sensor shear response and minimize its pressure response may help in effective design of direct shear stress sensors.

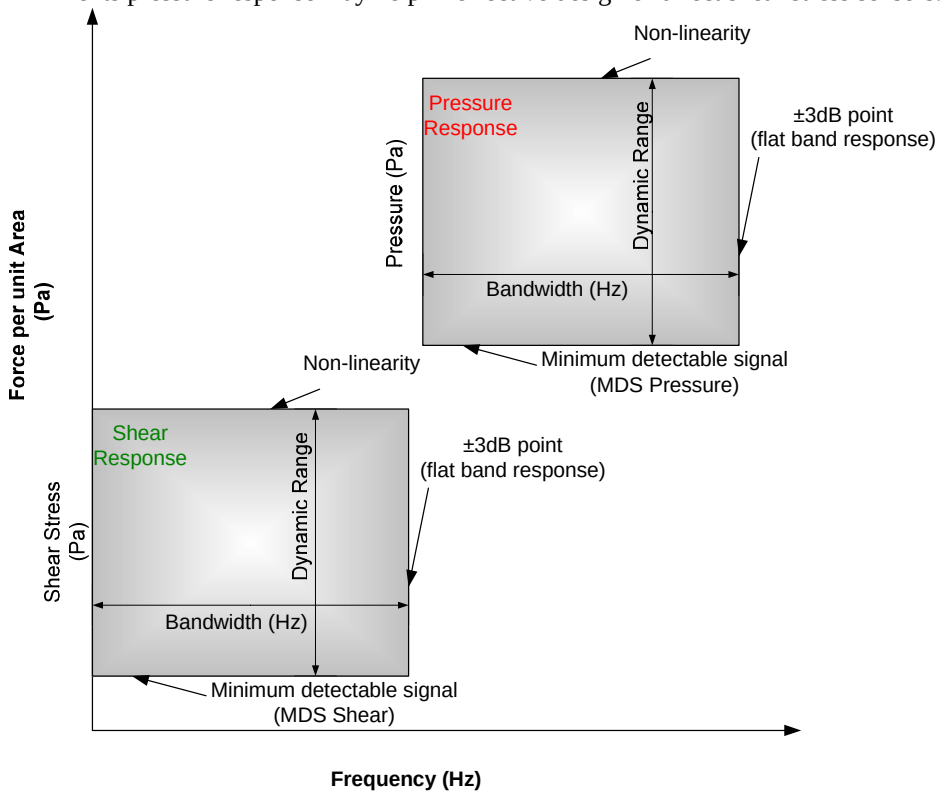

Figure 12 Schematic indicating desirable region of operation for floating element shear stress sensor under both shear and pressure forcing.

V. Conclusions

Dynamic pressure response of a micromachined differential capacitive direct shear stress sensor was investigated. The sensor possessed a linear sensitivity of $7.66\,mV/Pa$, a bandwidth of $6.2\,kHz$, a dynamic range $>102\,dB$, an MDS of $14.9\,\mu Pa$ at $1\,kHz$, and demonstrated pressure rejection of $64\,dB$. Experimental study indicates that the sensor pressure response affects shear measurement accuracy despite high pressure rejection. Pressure response shapes the combined shear-pressure frequency response of the sensor. Design considerations for estimating the pressure response of a micromachined capacitive shear stress sensor were presented. A combination of fluidic, mechanical, and electronic techniques for mitigation of sensor pressure response is suggested. An optimal design strategy for enhancing shear stress sensor performance while minimizing its pressure response is also provided.

VI. Acknowledgements

This work is funded by NASA Langley Research Center, Award # NNX07AB27A and monitored by Catherine B. McGinley. This project was also partially funded by the Florida Center for Advanced Aero-Propulsion (FCAAP).

References

1. Oudheusden, B. and Huijsing, J., "Integrated Flow Friction Sensor." *Sensors and Actuators A*, Vol. 15, No. 1988, pp. 135-144.
2. Kalvesten, E., Stemme, G., Vieider, C. and Lofdahl, L., "An Integrated Pressure-Flow Sensor for Correlation Measurement in Turbulent Gas Flow." *Sensors and Actuators A*, Vol. 52, No. 1996, pp. 51-58.
3. Liu, C., et al., "Micromachined flow shear-stress sensor based on thermal transfer principles." *Journal of Microelectromechanical Systems*, Vol. 8, No. 1, 1999, pp. 90-99.
4. Sheplak, M., Chandrasekaran, V., Cain, A., Nishida, T. and Cattafesta, L.N., "Characterization of a silicon-micromachined thermal shear-stress sensor." *AIAA Journal*, Vol. 40, No. 6, 2002, pp. 1099-1104.
5. von Papen, T., Steffes, H., Ngo, H.D. and Obermeier, E., "A micro surface fence probe for the application in flow reversal areas." *Sensors and Actuators A: Physical*, Vol. 97-98, No. 2002, pp. 264-270.
6. Große, S. and Schroder, W., "Mean wall-shear stress measurements using the micro-pillar shear-stress sensor MPS3." *Measurement Science & Technology*, Vol. 19, No. 1, 2008, pp. 12.
7. Große, S. and Schröder, W., "Dynamic wall-shear stress measurements in turbulent pipe flow using the micro-pillar sensor MPS3." *International Journal of Heat and Fluid Flow*, Vol. 29, No. 3, 2008, pp. 830-840.
8. Fourguette, D., et al., "Miniature and MOEMS Flow Sensor." *AIAA paper, 2001-2982*, Vol. No. 2001, pp. 12.
9. Gharib, M., Modarress, D., Fourguette, D. and Wilson, D. Optical Microsensors for Fluid Flow Diagnostics. in *AIAA Aerospace Sciences Meeting and Exhibit, 40th, #AIAA-2002-252* Reno, NV, 2002
10. Schmidt, M.A., Howe, R.T., S.D.Senturia and Haritonidis, J.H., "Design and Calibration of a Micromachined Floating-Element Shear-Stress Sensor." *Transactions of Electron Devices*, Vol. Ed-35, No. 1988, pp. 750-757.
11. Pan, T., Hyman, D. and Mehregany, M., "Microfabricated Shear Stress Sensors, Part 1:Design and Fabrication." *AIAA Journal*, Vol. Vol.37, No. No.1, 1999, pp. 66-72.
12. Hyman, D., Pan, T., Reshotko, E. and Mehregany, M., "Microfabricated shear stress sensors, Part 2: Testing and calibration." *AIAA Journal*, Vol. 37, No. 1, 1999, pp. 73-78.
13. Tiliakos, N., et al. A MEMS-based shear stress sensor for high temperature applications. in *46th AIAA Aerospace Sciences Meeting and Exhibit, #2008-274*, Reno, NV, 2008
14. Desai, A.V. and Haque, M.A., "Design and fabrication of a direction sensitive MEMS shear stress sensor with high spatial and temporal resolution." *Journal of Micromechanics and Microengineering*, Vol. 14, No. 12, 2004, pp. 1718.
15. Zhe, J., Modi, V. and Farmer, K.R., "A microfabricated wall shear-stress sensor with capacitative sensing." *Journal Of Microelectromechanical Systems*, Vol. 14, No. 1, 2005, pp. 167-175.
16. Chandrasekharan, V., Sells, J., Meloy, J., Arnold, D.P. and Sheplak, M. A Metal-On-Silicon Differential Capacitive Shear Stress Sensor. in *Transducers 2009, Technical Digest, 15th International Conference Solid State Sensors, Actuators, and Microsystems* Denver, CO, 2009
17. Padmanabhan, A., Goldberg, H., Breuer, K.D. and A.Schmidt, M., "A Wafer-Bonded Floating-Element Shear Stress Microsensor with Optical Position Sensing by Photodiodes." *J.Microelectromechanical Syst.*, Vol. 5, No. 4, 1996, pp. 307-315.
18. Padmanabhan, A., Sheplak, M., Breuer, K.D. and A.Schmidt, M., "Micromachined Sensors for Static and Dynamic Shear Stress Measurements in Aerodynamic Flows." *Technical Digest, Transducers '97, Chicago, IL*, Vol. No. 1997, pp. 137-140.
19. Tseng, F.-G. and Lin, C.-J., "Polymer MEMS-Based Fabry–Perot Shear Stress Sensor." *IEEE Sensors Journal*, Vol. 3, No. 6, 2003, pp. 812-817.
20. Horowitz, S., et al. A micromachined geometric moire interferometric floating element shear stress sensor. in *42nd AIAA Aerospace Sciences Meeting and Exhibit, # 2004-1042*, Reno, NV, 2004
21. Shajii, J., Ng, K.-Y. and A.Schmidt, M., "A Microfabricated Floating Element Shear Stress Sensor Using Wafer-bonding Technology." *Journal of Microelectromechanical Systems*, Vol. 1, No. 2, 1992, pp. 89-94.

22. Goldberg, H.D., Breuer, K.S. and Schmidt, M.A., "A Silicon Wafer-Bonding Technology for Microfabricated Shear-Stress Sensors with Backside Contacts." *Technology Digest, Solid-State Sensor and Actuator Workshop*, Vol. No. 1994, pp. 111-115.
23. Li, Y., et al. A MEMS shear stress sensor for turbulence measurements in *46th AIAA Aerospace Sciences Meeting and Exhibit, # AIAA-2008-269* Reno, NV, 2008
24. Barlian, A.A., Park, S.J., Mukundan, V. and Pruitt, B.L., "Design and characterization of microfabricated piezoresistive floating element-based shear stress sensors." *Sensors and Actuators a-Physical*, Vol. 134, No. 1, 2007, pp. 77-87.
25. Hu, Z.W., Morfey, C.L. and Sandham, N.D., "Wall pressure and shear stress spectra from direct simulations of channel flow." *AIAA Journal*, Vol. 44, No. 7, 2006, pp. 1541-1549.
26. Naughton, J.W. and Sheplak, M., "Modern Development in Shear Stress Measurement." *Progress in Aerospace Science*, Vol. 38, No. 2002, pp. 515-570.
27. Senturia, S.D., *Microsystem design*. 2001, Kluwer Academic Publishers: Boston. p. 142-145.
28. Loeppert, P.V. and Lee, S.B. SiSonic™ - The first commercialized MEMS microphone. in *Solid-State Sensors, Actuators, and Microsystems Workshop*, Hilton Head, SC, 2006.pp.27-30
29. Chandrasekharan, V., Sells, J., Arnold, D.P. and Sheplak, M. Characterization of MEMS-Based Floating Element Shear Stress Sensor. in *47th AIAA Aerospace Sciences Meeting and Exhibit, # AIAA 2009-316*, Orlando, 2009
30. Starr, J.B. Squeeze-film damping in solid-state accelerometers. in *Solid-State Sensor and Actuator Workshop, 1990. 4th Technical Digest., IEEE*, 1990.pp.44-47
31. Darling, R.B., Hivick, C. and Xu, J.Y., "Compact analytical modeling of squeeze film damping with arbitrary venting conditions using a Green's function approach." *Sensors and Actuators a-Physical*, Vol. 70, No. 1-2, 1998, pp. 32-41.
32. Bao, M.H., Yang, H., Sun, Y.C. and French, P.J., "Modified Reynolds' equation and analytical analysis of squeeze-film air damping of perforated structures." *Journal of Micromechanics and Microengineering*, Vol. 13, No. 6, 2003, pp. 795-800.
33. Chandrasekaran, V., Cain, A., Nishida, T., Cattafesta, L.N. and Sheplak, M., "Dynamic calibration technique for thermal shear-stress sensors with mean flow." *Experiments in Fluids*, Vol. 39, No. 1, 2005, pp. 56-65.